RSC Advances

PAPER

View Article Online
View Journal | View Issue

Cite this: *RSC Adv.*, 2021, **11**, 32143

Formulation of re-dispersible dry o/w emulsions using cellulose nanocrystals decorated with metal/metal oxide nanoparticles

Tharwat I. Shaheen *[a] and Isabelle Capron [b]

This study describes for the first time the preparation of re-dispersible surfactant-free dry eicosane oil emulsion using cellulose nanocrystals (CNCs) using the freeze-drying technique. Surface properties of CNCs constitute a critical point for the stability of o/w emulsions and thus can affect both the droplet size and dispersion properties of the emulsion. Therefore, surface modification of CNCs was performed to understand its effect on the size of the obtained re-dispersible dry o/w eicosane emulsion. Decoration of the CNC surface with metal and metal oxide nanoparticles was conducted through the available alcoholic groups of glycosidic units of CNC, which played a dual role in reducing and stabilizing nanoparticles. Of these nanoparticles, silver (AgNPs), gold (AuNPs), copper oxide (CuO-NPs), and iron oxide (Fe_3O_4-NPs) nanoparticles were prepared *via* a facile route using alkali activated CNCs. Thorough characterizations pertaining to the as-prepared nanoparticles and their re-dispersible dry eicosane o/w emulsions were investigated using UV-vis spectroscopy, TEM, XRD, particle size, zeta potential, and STEM. Results confirmed the ability of CNCs to stabilize and/or reduce the formed nanoparticles with different sizes and shapes. These nanoparticles showed different shapes and surface charges accompanied by individual morphologies, reflecting on the stability of the re-dispersed dry eicosane emulsions with droplet sizes varying from 1.25 to 0.5 μm.

Received 10th August 2021
Accepted 13th September 2021

DOI: 10.1039/d1ra06054f

rsc.li/rsc-advances

1. Introduction

Dry emulsions, as one of the recent pharmaceutical tools, have increasingly drawn the awareness of researchers. This is because their unique features gather together the advantages of lipid-based systems, such as lipophilic drug solubilization and physical stability of classic oil/water (o/w) emulsions.[1,2] Dry emulsions are systems generally formed by the removal of the aqueous phase of a liquid emulsion containing a water-soluble or insoluble solid carrier leaving behind a dispersion of the immiscible oil phase within a solid phase.[3] Because of the high rate of production, dried emulsions have a wide range of applications, especially in cosmetic, pharmaceutical, and food industries, in order to avoid oxidation reactions. This process of dehydration of emulsions enables the inclusion of antioxidants, organic compounds, and hydrophobic drugs into emulsions enabling them with the desirable antioxidant stability, color, and flavors.[4] Two basic routes are available to dry Pickering emulsion, typically, spray dry and freeze dry techniques, which are routinely used in this regard.[4,5] Contrary to spray drying, the freeze drying technique was successfully utilized for drying and re-dispersion of o/w emulsions. Unlike freeze drying, the rapid rate of dehydration of emulsion by the spray drying technique often causes disruption of the formed emulsion droplets, and thus, oil leakage takes place.[6] However, crystallization of water and oil droplets upon freezing may affect the stabilization of Pickering o/w emulsions, which leads to the coalescence of droplets.[7,8]

Most recently, Pickering emulsion has been stabilized by a wide variety of inorganic and organic colloidal nanoparticles, *e.g.*, silica, clay, starch, chitin, and CNC, as an alternative approach instead of conventional surfactants or as an additional stabilizer for ultra-stable Pickering o/w emulsions.[9–11] Among these nanoparticles, the use of biopolymers with environmental sustainability, low cost, and low energy consumption is ideally positioned for innovative strategy.[12,13] Notably, cellulose nanocrystal (CNC) can be irreversibly adsorbed at the water–oil interface.[14] As a result, CNC has been effectively used for developing o/w emulsions highly resistant to coalescence, creaming, or sedimentation[11,15] and through emulsion gels or emulgels.[16] Rod-like shaped CNC can be obtained from cellulose biomass such as wood and cotton by the acid hydrolysis process, generally with sulfuric acid in which the less ordered amorphous region is dissolved. It results in nanorods (150–200 nm long and 6–25 nm large) forming nanocrystals that are highly stable in water. The substantial stability of the colloidal suspension of CNC is due to the presence of negatively charged

[a]*National Research Centre (Scopus affiliation ID 60014618), Textile Industries Research Division, (former El-Tahrir str.), Dokki, P.O. 12622, Giza, Egypt. E-mail: shaheen_chem@yahoo.com*

[b]*INRAE, UR1268 Biopolymeres Interactions Assemblages, 44316 Nantes, France*

sulfate ester groups on the CNC surface, preventing aggregation by electrostatic repulsion.[17–22] It has been demonstrated in previous works that the low surface charge density of CNC ($\leq$0.03 e nm^{-2}) is critical to stabilizing o/w emulsion effectively, or this can introduce ionic strength to reduce repulsion.[23] CNC adsorbs at the interface forming highly stable droplets by the formation of a dense 2D network architecture.[11] Some modifications, such as graft polymerization of poly N-isopropyl acrylamide[24] or on CNC surface, improved the stability of emulsions without phase separation for more than four months.[25] In this context, the surface properties of CNC influence the interface behavior of the Pickering o/w emulsion. Therefore, the stabilization of droplets to coalescence can be managed by controlling surface properties.[26,27] Owing to the high density of hydroxyl groups on CNC surfaces, CNC has been integrated with different organic and inorganic hybrid nanoparticles. Special interest has been given to inorganic metals and metal oxides due to their unique physicochemical properties, which induce new CNC/nanohybrid members. Of these inorganic nanohybrids, Ag, Au, ZnO, and SiO_2 nanoparticles were synthesized through different approaches for applying in different state-of-the-art applications *e.g.*, water purification, tissue culture, supercapacitors, and catalysis.[12]

This study describes, for the first time, the development of re-dispersible Pickering dry o/w emulsion of eicosane oil stabilized CNC with and without surface decoration with inorganic metal/metal oxide nanoparticles. Eicosane is one of the most common paraffin hydrocarbons that can be employed in versatile applications, particularly in thermal energy storage.[28,29] Because eicosane has a melting temperature range of 35–37 °C, there is a phase change from solid at room temperature to liquid at near 37 °C.[30] Besides, due to its low melting vapor pressure, non-corrosive, nonhygroscopic, chemically, and thermally stable properties, eicosane is nominated as a model of oil phase for the preparation of dry o/w emulsions. We aimed to investigate the influence of surface decoration of CNC on the size of the droplet after re-dispersion in water as compared to an unmodified surface. To achieve this goal, surface decoration of CNC with silver nanoparticles (AgNPs), gold nanoparticles (AuNPs), copper oxide nanoparticles (CuO-NPs), and iron oxide nanoparticles (Fe_3O_4-NPs) were achieved through a novel facile route *via* harnessing the previously mentioned dual role properties of CNC as reducing and capping agents[22,31,32] except CuO-NPs, where CNC manifested as a capping agent. Such dry eicosane emulsions, stabilized by CNC and CNC/NPs, can serve as novel precursors for many applications, including medical, catalytic, and energy storage.

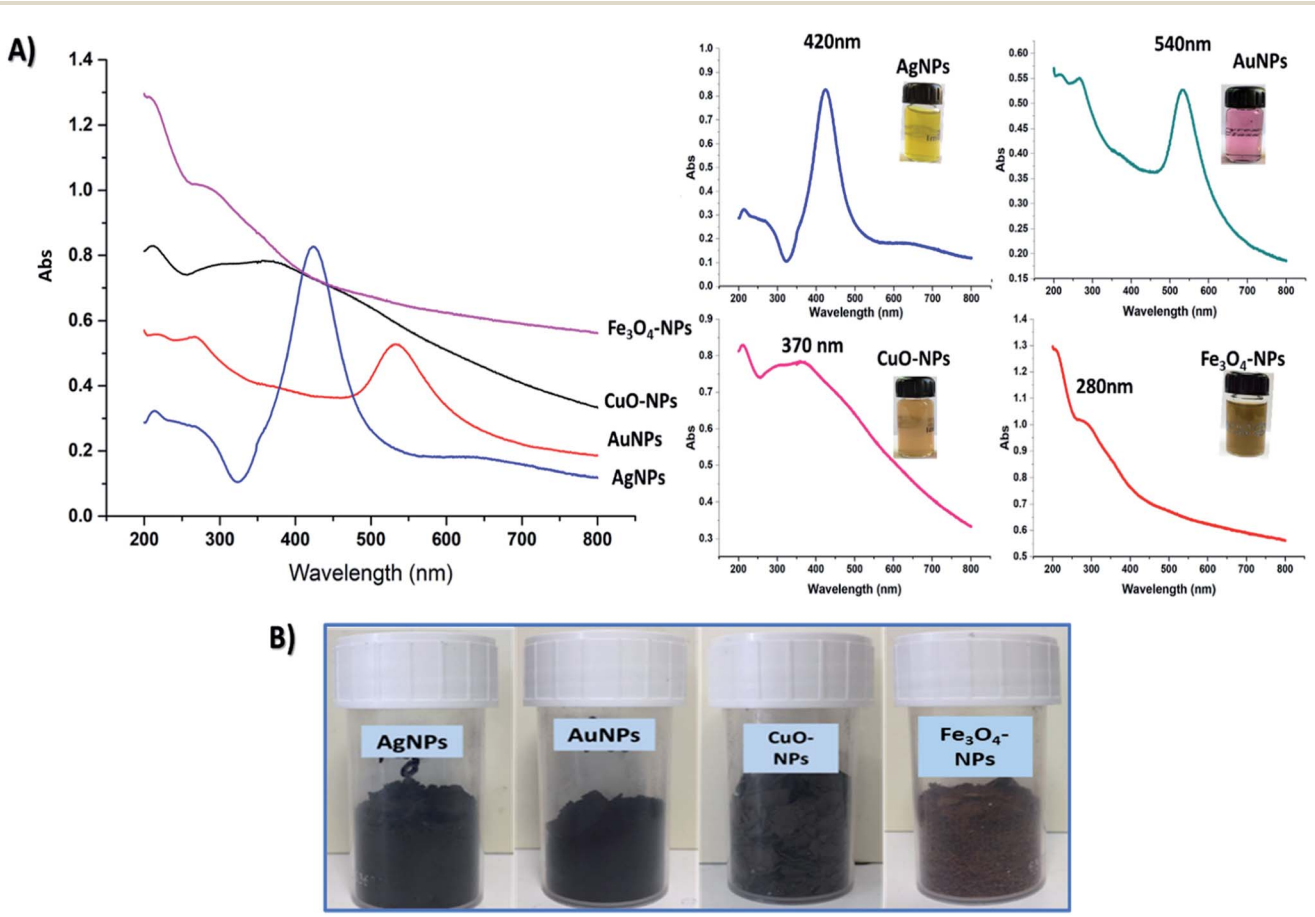

Fig. 1 UV-vis spectroscopy for nanoparticle decorated CNC (left side); images attached with the individual UV-vis spectra (right side) showed the color of the formed nanoparticles (A), corresponding pictures of nanoparticles after collecting by centrifuge and drying in an oven at 90 °C (B).

2. Experimental

2.1. Materials

CNC was supplied from Celluforce, Inc. and was used as received. The oil phase, eicosane (99%), was purchased from Sigma Aldrich. For nanoparticle preparation, silver nitrate ($AgNO_3$), hydrogen tetrachloroaurate ($HAuCl_4 \cdot 3H_2O$), copper sulfate ($CuSO_4 \cdot 5H_2O$), ferric chloride ($FeCl_3 \cdot 6H_2O$), ferrous sulfate ($FeSO_4 \cdot 7H_2O$), and sodium hydroxide (NaOH) were also purchased from Sigma–Aldrich. Water used in all experiments was purified with the Milli-Q reagent system (Millipore).

2.2. Preparation of metals/metal oxide nanoparticles

CNC was used to prepare metal nanoparticles, *e.g.*, AgNPs, AuNPs, and metal oxides, *e.g.*, Fe_3O_4-NPs and CuO-NPs, through a simple reaction with metals salts at a temperature of 60 °C for 30 min. CNC (0.2 g) was firstly re-suspended in 100 mL H_2O fixed at pH 12 using NaOH. For AgNPs, AuNPs, and CuO-NPs preparation, a final concentration of each $AgNO_3$ (1.0 mM), $AuCl^{3+}$ (1.0 mM), and $CuSO_4 \cdot 5H_2O$ (25 mM) were added, separately, to the suspension of CNC. While, in the case of Fe_3O_4-NPs, a mixture of $FeCl_3 \cdot 6H_2O$ and $FeSO_4 \cdot 7H_2O$ (ratio Fe^{3+} : Fe^{2+} = 25 mM : 55 mM) was firstly dissolved prior to adding to the CNC suspension. At the end of the reaction, the obtained nanoparticles were collected by centrifugation at 5000 rpm for 20 min and then dried at 90 °C in an oven.

2.3. Preparation of re-dispersible dry o/w emulsion

Dry oil/water emulsions were prepared using eicosane (oil liquid phase), and the CNC nanoparticles were uncoated or coated with metals and metal oxides at an equal ratio. Typically, 30 mg of eicosane was melted with 30 mg of the dried nanoparticles in separate plastic vials, and then 1.2 mL of the warmed distilled water at 40 °C to match an oil/water ratio of 20 : 80 was added to each mixture under a vortex shaker until homogeneity. Afterwards, mixtures were sonicated for 20 s with an ultrasonic device with a dipping titanium probe close to the surface using intermittent pulses (amplitude 2 corresponding to 4 W mL^{-1} applied power, 1 s pulse ON, 1 s pulse OFF). Finally, mixtures were frozen and dried in the freeze-dryer.

2.4. Characterizations

2.4.1 Ultraviolet-visible (UV-vis) spectroscopy. The formation of nanoparticles was monitored routinely with the aid of UV-vis spectroscopy. Samples were dispersed in distilled water (1 : 500 g mL^{-1}) and sonicated for 10 min before measurement. The spectra of the surface plasmon resonances of nanoparticles were screened using a Cary 100 UV-vis spectrophotometer in the range of 200–800 nm.

2.4.2 Transmission electron microscopy (TEM). Surface morphologies of the prepared AgNPs, AuNPs, CuO-NPs, and Fe_3O_4-NPs were visualized through TEM. Colloidal solutions of nanoparticles were deposited on fresh glow discharged carbon coated copper grids (Electron Microscopy Sciences, UK) for 2 min, and the excess was removed by blotting. The sample was observed under standard conditions using a JEOL JEM-1230 TEM at 80 kV.

2.4.3 Dynamic light scattering (DLS) and zeta potential. Both narrow particle size distribution and the accumulated surface charges (zeta potential value) of the formed hybrid nanoparticles were determined through a Malvern Zetasizer

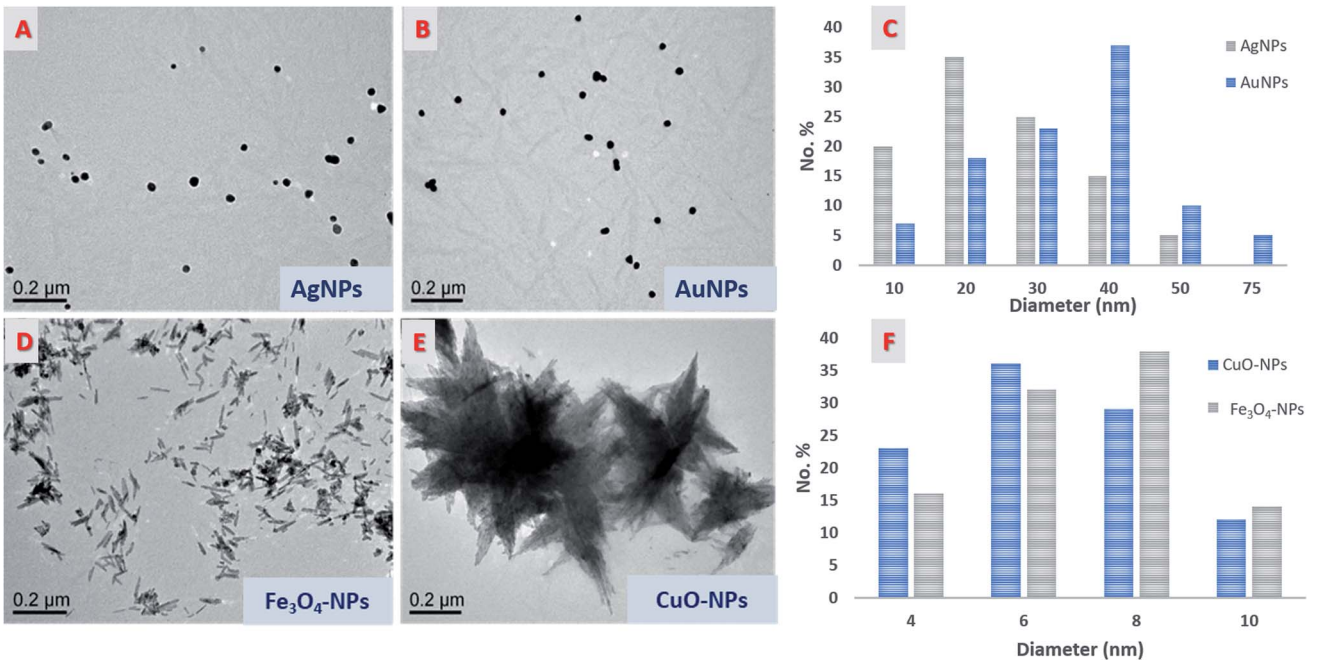

Fig. 2 TEM micrographs of nanoparticles (A, B, D, and E), histogram distribution of AgNPs and AuNPs (C), and histogram distribution of the mean width of CuO-NPs and Fe_3O_4-NPs (F).

Table 1 DLS and zeta potential results for the as-formed nanoparticles decorating CNC

Sample	*Z*-average (nm)	PDI	Peak (nm)	Zeta potential (mV)
CNC	80.8 ± 0.4	0.52 ± 0.02	154.0 ± 7.56	−43.4 ± 2.7
AgNPs/CNC	230.8 ± 4.6	0.40 ± 0.01	317.7 ± 10.8	−25.8 ± 0.5
AuNPs/CNC	153.9 ± 4.0	0.36 ± 0.02	223.1 ± 14.1	−27.1 ± 1.6
CuO-NPs/CNC	614.8 ± 3.6	0.12 ± 0.03	694.4 ± 30.8	−35.2 ± 2.7
Fe_3O_4-NPs/CNC	354.4 ± 5.8	0.25 ± 0.03	447.0 ± 44.4	−28.1 ± 0.8

(version 7.11). Suspensions were prepared at 0.3 g L^{-1}, dispersed with deionized water, and determined in triplicate.

2.4.4 X-ray diffraction patterns (XRD). XRD spectra were obtained for individual nanoparticles as well as their freeze-dried emulsions, and the data obtained from XRD were recorded every 10 min on a Bruker D8 Discover diffractometer. Cu-Kα1 radiation (Cu Kα1 = 1.5405 Å), produced in a sealed tube at 40 kV and 40 mA, was selected and parallelized using a Gobël mirror parallel optics system and collimated to produce a 500 μm beam diameter. The data were collected in the 2θ = 5–40° range.

2.4.5 Emulsion droplet size. Individual average droplet diameter of each emulsion after re-suspension was measured by laser light scattering using a Horiba LA-960 particle size distribution analyzer (Kyoto, Japan). An analysis model was used with the refractive indices of 1.44 and 1.33 for eicosane at 20 °C and water, respectively. The calibration for water as a reference was taken before each measurement. All emulsions were measured at a range of transmittance between 80 and 90%. The measurements were systematically carried out in triplicate. The diameter was expressed as surface mean diameter D (3,2) (the Sauter diameter).

2.4.6 Scanning transmission electron microscopy (STEM). The surface of the formulated dry emulsions was coated with platinum prior to visualization on a JEOL JSM-7600F field-emission STEM instrument.

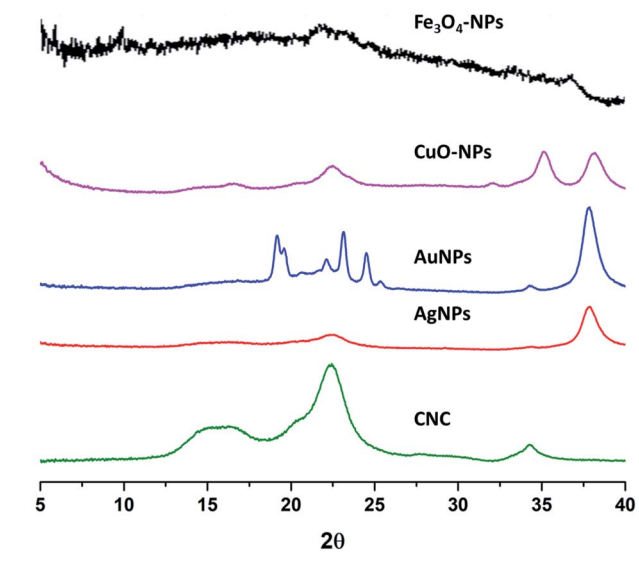

Fig. 3 XRD patterns of CNC, AgNPs, AuNPs, CuO-NPs, and Fe_3O_4-NPs.

3. Results and discussions

3.1. Preparation of nanoparticles decorating CNC

Four hybrid nanoparticles were prepared in this study by the use of CNC, which acted as reducing and stabilizing agents for assessing the formation of well stabilized metal and metal oxide nanoparticles. In an alkali medium, CNC promotes negatively charged groups on its surface that might play an important role in reducing the valency of metals. As previously mentioned, our technique is designed to activate the reducibility of CNC by creating negatively charged hydroxide groups (CH_2O^-) on the C6 position of glycosidic units, which in turn play a dual role in the reduction and stabilization of the formed nanoparticles.[22] The attraction between alkaline CNC and metal ions occurs through an adsorption mechanism prior to reduction. Typically, AgNPs, AuNPs, CuO-NPs, and Fe_3O_4-NPs were prepared from

Fig. 4 (A) Dry o/w emulsion of eicosane stabilized with different nanoparticles – from left to right – AgNPs, AuNPs, CuO-NPs, Fe_3O_4-NPs, and CNC; (B) o/w emulsion of eicosane stabilized with different nanoparticles (from left to right – AgNPs, AuNPs, CuO-NPs, and Fe_3O_4-NPs) after re-dispersion in distilled water (0.05 g mL^{-1}).

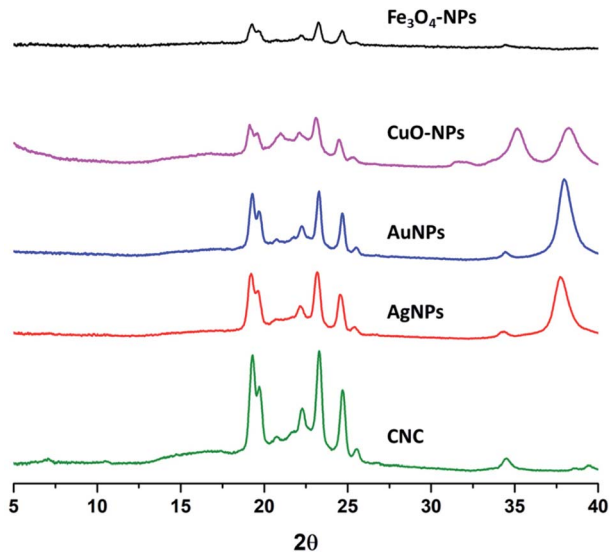

Fig. 5 XRD of dry eicosane o/w emulsions stabilized by CNC, AgNPs, AuNPs, CuO-NPs, and Fe_3O_4-NPs.

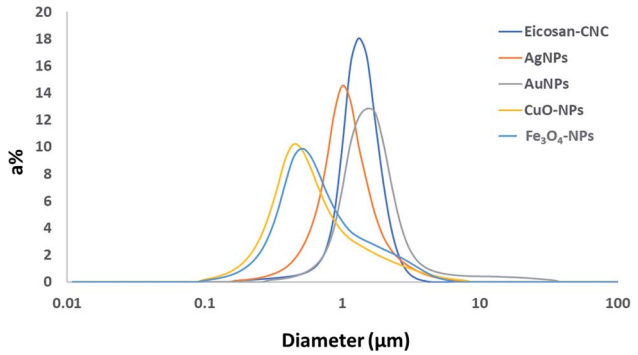

Fig. 6 Droplet size distributions of the prepared dry eicosane o/w emulsions stabilized by CNC with and without nanoparticle decoration after re-dispersion.

Table 2 Mean droplet diameter of dry eicosane o/w emulsions stabilized by CNC with and without nanoparticle decoration after re-dispersion and surface charge of the NPs determined by *Z*-potential

Stabilizer	Mean droplet diameter (μm)	Surface charge (mV)
CNC	1.25	−43.4 ± 2.7
AgNPs/CNC	0.98	−25.8 ± 0.5
AuNPs/CNC	1.46	−27.1 ± 1.6
CuO-NPs/CNC	0.50	−35.2 ± 2.7
Fe_3O_4-NPs/CNC	0.57	−28.1 ± 0.8

their salts, which are $AgNO_3$, $AuCl^{3+}$, $CuSO_4 \cdot 5H_2O$, and $FeCl_3 \cdot 6H_2O/FeSO_4 \cdot 7H_2O$, respectively. The reduction of metals is frequently accompanied by gradual changes in the color of solutions, referring to the formation of nanoparticles. At the end of the reaction, each metal and metal oxide appeared in a distinct color, which might be attributed to their surface plasmon resonance (SPR). UV-vis spectra and color of colloidal solutions of AgNPs, AuNPs, CuO-NPs, and Fe_3O_4-NPs are presented in Fig. 1A. Data represented in Fig. 1 show intense characteristics peaks at maximum absorption of 420 nm,[33] 540 nm,[34] 370 nm,[35,36] and 290 nm (ref. 37) for AgNPs, AuNPs, CuO-NPs, and Fe_3O_4-NPs, respectively. This clearly confirmed the successful formation of nanoparticles with a narrow size distribution. In addition, their colors in the solid state showed darker colors than in their colloidal suspension, as represented in Fig. 1B.

Noticeably, however, the color change of solutions indicates the reduction of nanoparticles.[38,39] Through free alcoholic hydroxyl groups attached on C6 of cellulose chains after alkali activation, the stability of the formed nanoparticles at the aforementioned preparation protocol, as well as their sizes and distributions, were investigated through TEM and particle size analyses. TEM images of nanoparticles were captured after re-suspension of nanoparticle powders in water and drying on a grid, separately.

Fig. 2 shows TEM images of prepared AgNPs, AuNPs, Fe_3O_4-NPs, and Cu-NPs (without stain). The form visualized with high contrast corresponds to the metallic NPs. This allows determining the shape and size of the formed nanoparticles. In the case of AgNPs and AuNPs metal nanoparticles, well-distributed spherical particles with an average diameter in the range of 20–50 nm were achieved. Despite the low contrast of CNC in TEM investigations, a CNC can be seen. It appears that NPs are fixed to the particles preventing them from aggregation and agglomeration.

On the contrary, Fe_3O_4-NPs and Cu-NPs exhibited a rod-like shape with two different rearrangements responsible for the formation of a flower shape, as in the case of CuO-NPs. In these cases, CNC cannot be seen even at high magnifications. These phenomena predicted that the reduction of metal oxide was carried out on the surface of CNC, causing deposition of the formed nanoparticles on its surface, and thereby, CNC acted as a scaffold for building a new rod shape with different rearrangements. The individual rods of both Fe_3O_4-NPs and Cu-NPs had a size above 100 nm in length while their width was in the range of 1–10 nm.

3.1.1 Hybrid particle dimensions. The size of re-suspended nanoparticles was analyzed by the DLS technique and is presented in Table 1. DLS is dedicated to the dispersion of spherical particles *d*. Consequently, for non-spherical particles such as CNC, the *Z*-average parameter determines a size equivalent to the hydrodynamic diameter of a sphere that diffuses at the same rate as non-spherical particles. Data given in Table 1 show a systematic increase in the size of CNC after surface decoration with metal oxide nanoparticles. This increase in CNC dimension was proportional to the peak picked at high peak intensity. However, the DLS *Z*-average sizes of both Fe_3O_4-NPs and CuO-NPs were larger than those obtained from AgNPs and AuNPs. As indicated from Table 1, all examined particles, even the larger ones, possessed a narrow size distribution with a polydispersity (PDI) lower than 0.7. In addition, surface decoration of CNC with nanoparticles decreased the accumulated negative charge on CNC as indicated from zeta potential values given in

Table 1. These results indicate a surface modification linked to the deposition of nanoparticles on the surface of CNC.

3.1.2 XRD analysis. XRD spectra of CNC and their surface decoration with nanoparticles are represented in Fig. 3. The spectra of CNC exhibited distinctive peaks at $2\theta = 15.1°$, 16.2°, 22.6°, and 34.5° assigned to (1−10), (110), (200), and (004) crystallographic planes of cellulose I,[18,19] respectively. For metal nanoparticles, both AgNPs and AuNPs spectra exhibited a new peak allocated at the same range of 38.4°, which corresponds to the (111) crystal plane of AgNPs and AuNPs.[40] However, small peaks close to 25° were observed that could be assigned to sodium chloride. In addition, the XRD spectrum of CuO-NPs showed new peaks at 35.6° and 38.8°, corresponding to (002) and (111) planes,[41] which proves the formation of monoclinic single phase CuO-NPs on the surface of CNC. While, the XRD spectrum of Fe_3O_4-NPs displayed noisy and humpy diffraction peaks, which could be due to the formation of very small nanoparticles deposited inside and on CNC, causing a layer of native oxides that cover the surface of CNC. However, the XRD pattern of Fe_3O_4-NPs showed low intensity broad peaks at 30° and 36°, corresponding to Fe_3O_4 indices (220) and (311).[40]

3.2. Preparation of dry o/w emulsion

Eicosane in the o/w emulsion was stabilized using CNC with and without surface decoration of nanoparticles after sonication for 20 s. Equal ratios (30 mg) of both eicosane and CNC

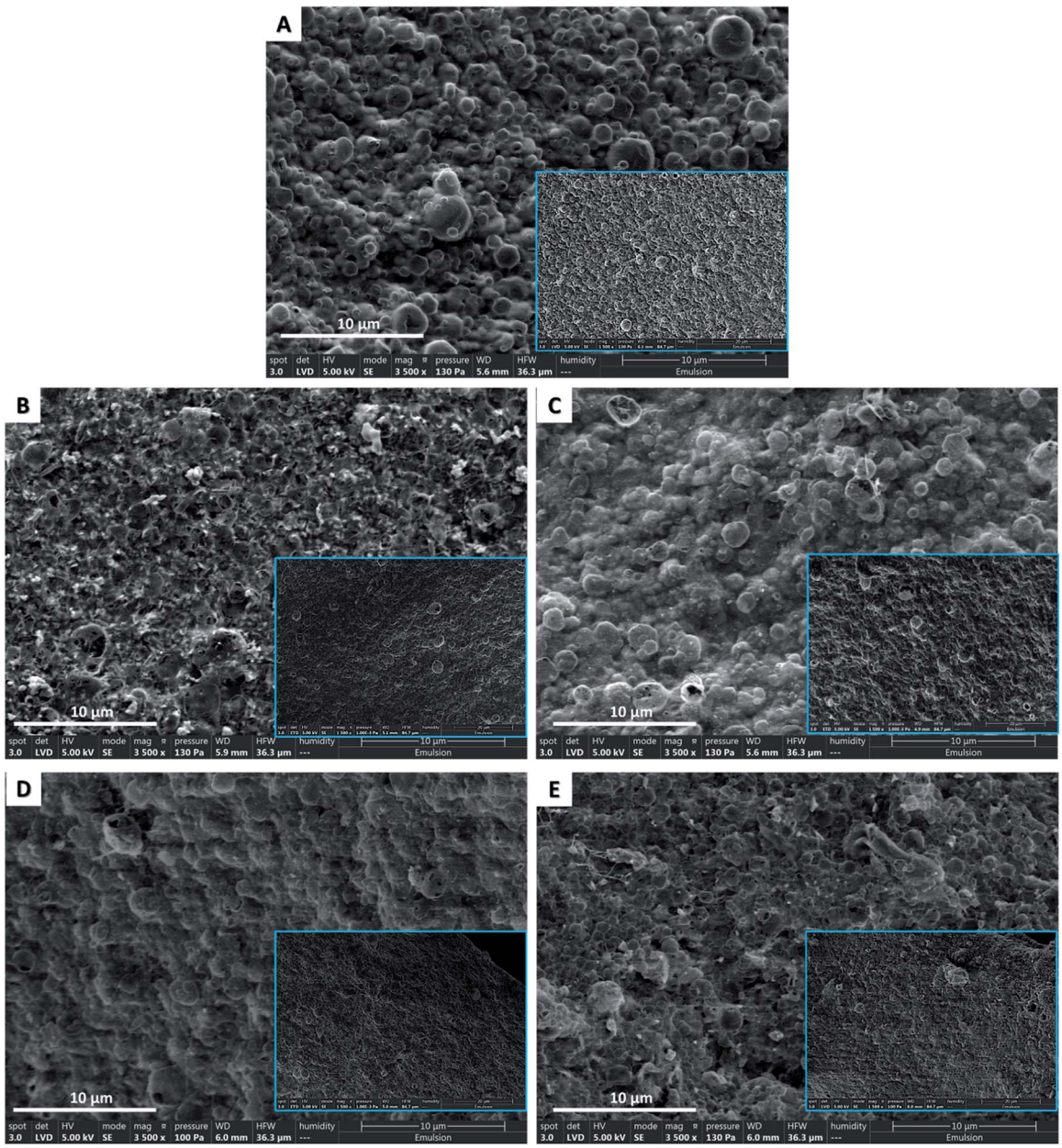

Fig. 7 STEM micrographs (3500× magnification) for dry eicosane o/w emulsion stabilized by CNC (A), AgNPs (B), AuNPs (C), CuO-NPs (D), and Fe_3O_4-NPs (E). Small pictures correspond to 1500× magnification.

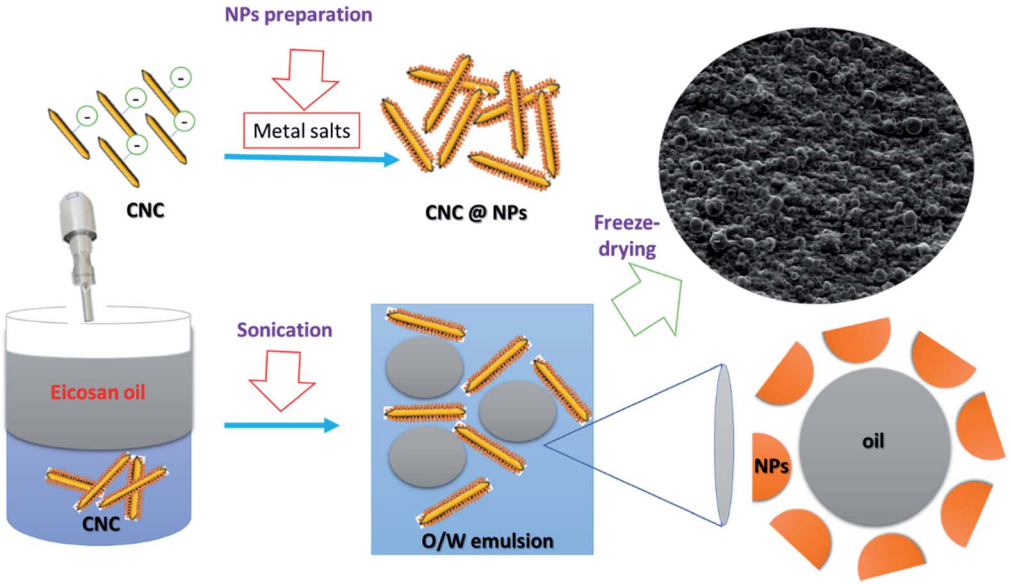

Scheme 1 A diagram for preparation of dry eicosane o/w emulsion.

alone or decorated with different nanoparticles were applied. Typically, two different metal nanoparticles *versus* the other two different metal oxide nanoparticles were used in order to investigate their ability to stabilize the formed emulsion as a function of droplet size and surface charges. The prepared emulsions were frozen, and only the water was easily removed, undergoing a freeze drier step without any changes in the formed emulsions when small portions of the dry emulsions were re-dispersed again in water by slight sonication for 5 s to ensure full dispersion as seen from Fig. 4. Visually, the dried emulsions kept their own color after re-dispersion in water, forming o/w emulsions with high homogeneity and stability for more than 2 weeks and did not get disrupted by centrifugation at 5000 rpm.

On the other hand, XRD patterns of dry eicosane emulsions were also investigated, and the spectra are presented in Fig. 5. In comparison with the XRD patterns of NPs (Fig. 3), the presence of characteristic peaks assigned to crystal plane (200) from CNC and crystal plane (111) from NPs can be distinguished, which are accompanied by new sharp peaks from eicosane allocated at 19.6°, 19.9°, 23.5°, 24.8°, and 25.6°, corresponding to the (010), (011), (105), (101), and (110) *n*-eicosane β phase crystal planes, respectively, agreeing with the standard PDF card of eicosane no. 45-1543.[42] Therefore, Fig. 5 emphasized the presence of CNC decorated NPs in dry eicosane o/w emulsion.

Furthermore, the droplet size distribution of the obtained emulsions is shown in Fig. 6, and the mean droplet sizes are summarized in Table 2.

Results obtained from Fig. 6 compared the effect of different types of nanoparticles applied in the stabilization of eicosane emulsion to native CNC. The mean average diameter of 1.25 μm after re-dispersion in the case of CNC shows the significance of the applied redispersion ratio of oil : CNC : water (1 : 1 : 20) in the successful preparation of smaller emulsion droplet sizes as compared with the droplet size obtained from other reports,[23,43] where CNC was used without the drying step. For nanoparticles, the droplet size of the emulsion was even reduced with varying the nanoparticles attached with CNC, except in AuNPs. Among the nanoparticles used, both CuO-NPs and Fe_3O_4-NPs reduced the droplet size to attain the smallest mean average size at 0.5–0.6 μm. It is worth noting that the shape and zeta potential of NPs stabilizing the interface are recognized as the main factors that might affect emulsion stability. Shape anisotropy can effectively promote emulsion stability by affecting the packing density of particles and interfacial capillary interactions at the oil/water interface.[44,45] Lowering the surface zeta potential of NPs possibly reduces the repulsion as their decreasing hydrophilic character facilitates their adsorption at the oil/water interface.[46] The anisotropic shapes of CuO-NPs and Fe_3O_4-NPs played a crucial role in the stabilization and reduction of the emulsion droplet size. In addition, modifying the surface chemistry of NPs also changes the surface chemistry of the doplets. The tendency to aggregate may produce surface reinforcement or flocculation that enhances the stability of emulsions by saturating the surface of droplets with densely packed NPs.

3.2.1 STEM analysis on the dry emulsion. Dry eicosane droplets can be visualized for their droplet size by employing the STEM analysis, as shown in Fig. 7.

STEM images showed that the dry emulsions appeared as outstanding bumps that were the oil droplets. This evidence affirmed definitely that both CNC and their decorated nanoparticles, AgNPs, AuNPs, CuO-NPs, and Fe_3O_4-NPs, are capable of stabilizing eicosane o/w emulsion in the dry state. Interestingly, all the dry oil droplets manifested with uniform distribution and near round shapes after freeze-drying and were still covered with CNC/nanoparticles without any rupture. Micrographs also indicated the presence of nanoparticles (as bright spots) surrounding the dry droplets of eicosane. However, the decorated CNC stabilizes eicosane o/w emulsions in the small

droplet size ranging from 1.5–0.4 μm. More precisely, CuO-NPs and Fe_3O_4-NPs presented dry droplets with smaller sizes than those from AgNPs and AuNPs, which could be attributed to the low surface charge density. These findings emphasized that the freeze-drying approach is an effective way to avoid further rupture as it is a gentle drying technique. Scheme 1 represented the possible mechanism for nanoparticle decoration and emulsion formation.

4. Conclusion

New re-dispersible dry eicosane o/w emulsions were successfully fabricated using CNC as a stabilizer with an average droplet size of around 1.25 μm using the freeze-drying technique. Surface decoration of CNC was also achieved *via* the deposition of different metals and metal oxide nanoparticles on CNC. All of these nanoparticles were prepared by employing alkali activated CNC as capping and/or reducing agents. In particular, AgNPs, AuNPs, CuO-NPs, and Fe_3O_4-NPs were successfully fabricated and characterized using TEM, XRD, and a particle size analyzer. By the reduction of surface charge densities through the chemical decoration of CNC with metal and metal oxide nanoparticles, the droplet size of the formed dry emulsions after re-dispersion was decreased to attain the smallest size at 0.5 μm as deduced from granulometry and STEM images of CuO-NPs and Fe_3O_4-NPs stabilized o/w eicosane emulsions. Therefore, it is conceivable to fabricate stable re-dispersible dry o/w eicosane emulsions with various properties and controllable droplet diameters ranging from 1.5–0.4 μm by modifying CNC and its decorated surface with nanoparticles.

Conflicts of interest

There are no conflicts to declare.

Acknowledgements

This work was carried out in the framework of cooperation between STDF, Egypt Grant No. 25275 and Biopolymères Interactions Assemblages, INRAE, 44316 Nantes, France. We are equally grateful to Emilie Perrin and Joëlle Davy for their excellent technical assistance for TEM and SEM visualizations, Genevieve Llamas for granulometry, and Bruno Pontoire for XRD analysis. Also, Tharwat I. Shaheen would like to express his deep thanks to all the INRAE family, with special thanks to I. Capron for her support, guidance, time, and effective dedicated efforts.

References

1 M. Pohlen, Z. Lavrič, C. Prestidge and R. Dreu, *AAPS PharmSciTech*, 2020, **21**, 1–19.
2 A. Tan, S. Rao and C. A. Prestidge, *Pharm. Res.*, 2013, **30**, 2993–3017.
3 K. Christensen, G. Pedersen and H. Kristensen, *Int. J. Pharm.*, 2001, **212**, 187–194.
4 Y. Esparza, T.-D. Ngo and Y. Boluk, *Colloids Surf., A*, 2020, 124823.
5 A. Richter and K. Steiger-Trippi, *Pharm. Acta Helv.*, 1961, **36**, 322.
6 Z. Hu, H. S. Marway, H. Kasem, R. Pelton and E. D. Cranston, *ACS Macro Lett.*, 2016, **5**, 185–189.
7 Q. Zhu, Y. Pan, X. Jia, J. Li, M. Zhang and L. Yin, *Compr. Rev. Food Sci. Food Saf.*, 2019, **18**, 1660–1675.
8 B. M. Degner, C. Chung, V. Schlegel, R. Hutkins and D. J. McClements, *Compr. Rev. Food Sci. Food Saf.*, 2014, **13**, 98–113.
9 I. Capron and B. Cathala, *Biomacromolecules*, 2013, **14**, 291–296.
10 Y. Chevalier and M.-A. Bolzinger, *Colloids Surf., A*, 2013, **439**, 23–34.
11 I. Kalashnikova, H. Bizot, B. Cathala and I. Capron, *Langmuir*, 2011, **27**, 7471–7479.
12 E. Lizundia, D. Puglia, T.-D. Nguyen and I. Armentano, *Prog. Mater. Sci.*, 2020, **112**, 100668.
13 K. De France, Z. Zeng, T. Wu and G. Nyström, *Adv. Mater.*, 2020, 2000657.
14 S. A. Kedzior, V. A. Gabriel, M. A. Dubé and E. D. Cranston, *Adv. Mater.*, 2020, 2002404.
15 I. Capron, O. J. Rojas and R. Bordes, *Curr. Opin. Colloid Interface Sci.*, 2017, **29**, 83–95.
16 Z. Hu, T. Patten, R. Pelton and E. D. Cranston, *ACS Sustainable Chem. Eng.*, 2015, **3**, 1023–1031.
17 A. Hebeish, S. Farag, S. Sharaf and T. I. Shaheen, *Carbohydr. Polym.*, 2014, **102**, 159–166.
18 A. Hebeish, S. Farag, S. Sharaf and T. I. Shaheen, *Cellulose*, 2014, **21**, 3055–3071.
19 A. Hebeish, S. Farag, S. Sharaf and T. I. Shaheen, *Fibers Polym.*, 2015, **16**, 276–284.
20 A. Hebeish, S. Farag, S. Sharaf and T. I. Shaheen, *Int. J. Biol. Macromol.*, 2015, **81**, 356–361.
21 T. I. Shaheen and H. E. Emam, *Int. J. Biol. Macromol.*, 2018, **107**, 1599–1606.
22 T. I. Shaheen and A. Fouda, *Int. J. Biol. Macromol.*, 2018, **106**, 784–792.
23 I. Kalashnikova, H. Bizot, B. Cathala and I. Capron, *Biomacromolecules*, 2012, **13**, 267–275.
24 Z. Hu, R. M. Berry, R. Pelton and E. D. Cranston, *ACS Sustainable Chem. Eng.*, 2017, **5**, 5018–5026.
25 G. Sèbe, F. d. r. Ham-Pichavant and G. Pecastaings, *Biomacromolecules*, 2013, **14**, 2937–2944.
26 S. Fujisawa, E. Togawa and K. Kuroda, *Sci. Technol. Adv. Mater.*, 2017, **18**, 959–971.
27 D. Saidane, E. Perrin, F. Cherhal, F. Guellec and I. Capron, *Philos. Trans. R. Soc., A*, 2016, **374**, 20150139.
28 F. Wang, Y. Zhang, X. Li, B. Wang, X. Feng, H. Xu, Z. Mao and X. Sui, *Carbohydr. Polym.*, 2020, **234**, 115934.
29 F. Jiang, X. Wang and D. Wu, *Appl. Energy*, 2014, **134**, 456–468.
30 J. Y. Do, N. Son, J. Shin, R. K. Chava, S. W. Joo and M. Kang, *Mater. Des.*, 2021, **198**, 109357.
31 S. A. Ogundare and W. E. van Zyl, *Surf. Interfaces*, 2018, **13**, 1–10.

32 Z. Guo and S. Fu, *BioResources*, 2019, **14**, 3057–3068.
33 J. Sackey, A. Fell, J. B. Ngilirabanga, L. C. Razanamahandry, S. K. O. Ntwampe and M. Nkosi, *Mater. Today: Proc.*, 2021, **36**, 336–342.
34 P. K. Ngumbi, S. W. Mugo, J. M. Ngaruiya and C. K. King'ondu, *Mater. Chem. Phys.*, 2019, **233**, 263–266.
35 K. Pakzad, H. Alinezhad and M. Nasrollahzadeh, *Ceram. Int.*, 2019, **45**, 17173–17182.
36 T. I. Shaheen, A. Fouda and S. S. Salem, *Ind. Eng. Chem. Res.*, 2021, **60**(4), 1553–1563.
37 C. Justin, S. A. Philip and A. V. Samrot, *Appl. Nanosci.*, 2017, **7**, 463–475.
38 A. Zielińska, E. Skwarek, A. Zaleska, M. Gazda and J. Hupka, *Procedia Chem.*, 2009, **1**, 1560–1566.
39 J. Santhoshkumar, S. Rajeshkumar and S. Venkat Kumar, *Biochem. Biophys. Rep.*, 2017, **11**, 46–57.
40 M. Fahlepy and V. Tiwow, *J. Phys.: Conf. Ser.*, 2018, **997**(1), 012036.
41 P. Khanna, S. Gaikwad, P. Adhyapak, N. Singh and R. Marimuthu, *Mater. Lett.*, 2007, **61**, 4711–4714.
42 K. Sun, Y. Kou, H. Dong, S. Ye, D. Zhao, J. Liu and Q. Shi, *J. Mater. Chem. A*, 2021, **9**, 1213–1220.
43 S. Varanasi, L. Henzel, L. Mendoza, R. Prathapan, W. Batchelor, R. Tabor and G. Garnier, *Front. Chem.*, 2018, **6**, 409.
44 B. Madivala, S. Vandebril, J. Fransaer and J. Vermant, *Soft Matter*, 2009, **5**, 1717–1727.
45 J.-C. Loudet, A. M. Alsayed, J. Zhang and A. G. Yodh, *Phys. Rev. Lett.*, 2005, **94**, 018301.
46 B. P. Binks, J. A. Rodrigues and W. J. Frith, *Langmuir*, 2007, **23**, 3626–3636.